DFT Calculations of Triethyl and Trimethyl Orthoacetate Elimination Kinetics in the Gas Phase

Edgar Márquez,[†] José R. Mora,[†] Tania Cordova,[‡] and Gabriel Chuchani*[,†]

Centro de Química, Instituto Venezolano de Investigaciones Científicas (I.V.I.C.), Apartado 21827, Caracas, Venezuela, and Escuela de Química, Facultad de Ciencias, Universidad Central de Venezuela, Apartado 1020-A, Caracas, Venezuela

Received: December 9, 2008; Revised Manuscript Received: January 20, 2009

The reaction paths for the gas-phase molecular elimination of triethyl and trimethyl orthoesters were examined at B3LYP/6-31G(d,p), B3LYP/6-31G++(d,p), B3PW91/6-31G(d,p), B3PW91++G(d,p), MPW1PW91/6-31G(d,p), and MPW1PW91/6-31++G(d,p) levels of theory. The thermal decomposition of ethyl and methyl orthoesters involves similar transition state configurations in a four-membered ring arrangement. Products formed are ethanol and the corresponding unsaturated ketal for ethyl orthoesters, while in methyl orthoesters are methanol and the corresponding unsaturated ketal. Calculated thermodynamic and kinetic parameters from B3LYP calculations were found to be in good agreement with the experimental values. The calculated data imply the polarization of the C_3-O_4, in the direction $C_3^{\delta+}\cdots O_4^{\delta-}$, is rate determining. The NBO charges, bond indexes, and synchronicity parameters suggest the elimination reactions of ethyl orthoesters occur through a more polar asynchronic mechanism compared to methyl orthoesters.

I. Introduction

In 1922, Staudinger and Rathsam[1] reported the thermal decomposition of some triethyl orthoesters in a glass tube and in the presence of nickel in pumice stone at 250−260 °C producing diethyl ether and the corresponding ethyl ester (reaction II)

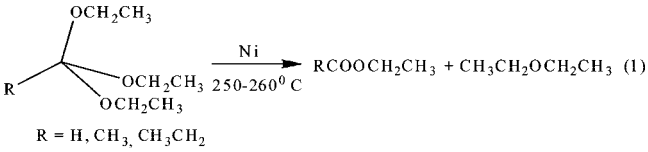

Moreover, distillation of triethyl orthophenylacetate from 85 to 86 °C at 0.5 mmHg was found to give ethyl phenyl acetate, ethanol, and corresponding phenyl ketene acetal (reaction II). These authors also proved that pure phenyl ketene diethyl acetal when heated in a high-pressure bomb at 260−270 °C yielded mainly ethyl phenylacetate, presumably ethylene gas, and an unidentified solid.

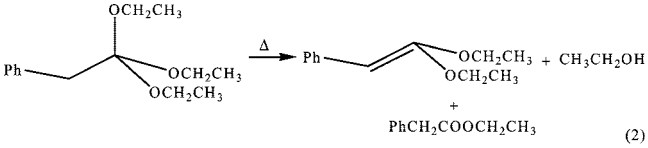

Triethyl orthobenzoate, which has no α-hydrogen, heated in a steel bomb was shown to give the normal ester and diethyl ether (reaction II).[2]

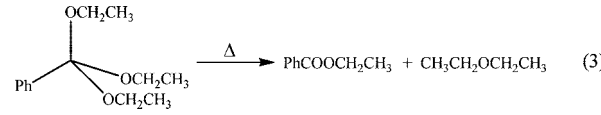

The substrate triethyl orthophenyl acetate through slow distillation gave phenyl ketene diethyl acetal and ethyl phenylacetate.[3] However, when trimethyl orthophenyl acetate was heated at 250−260 °C, the products were phenyl ketene dimethyl acetal and methyl phenylacetate. A vigorous evolution of methanol formation in the pyrolysis of the latter orthoester led to the belief of the interaction of two molecules of trimethyl orthophenyl acetate (reaction II).

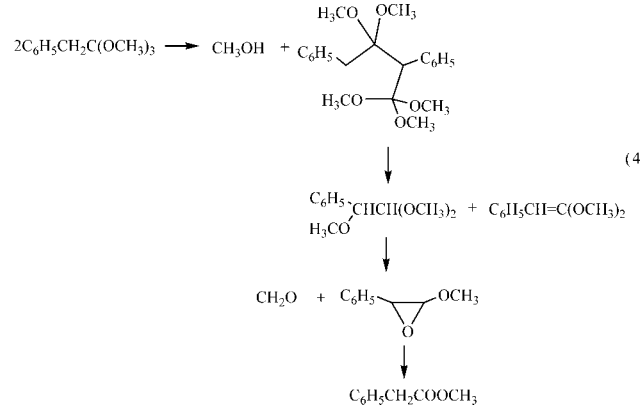

The small amount of information on the pyrolysis of organic orthoesters led to a recent examination of the homogeneous, unimolecular, gas phase elimination kinetics of triethyl and trimethyl orthoesters.[4,5] According to the experimental results of these works, the kinetic and thermodynamic parameters suggested the mechanistic decompositions of these reactions as depicted in reactions II and II.

* Corresponding author. E-mail: chuchani@ivic.ve.
[†] Instituto Venezolano de Investigaciones Científicas.
[‡] Universidad Central de Venezuela.

10.1021/jp8108336 CCC: $40.75
Published on Web 02/17/2009

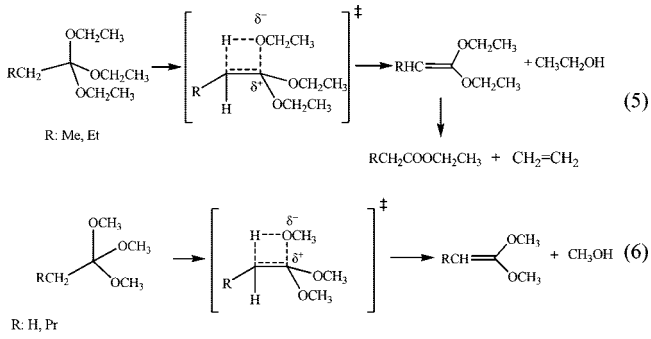

In order to gain more insight into the mechanisms of the gas phase thermal elimination of triethyl and trimethyl orthoesters, it seemed interesting to carry out a theoretical study at several computational levels in order to further our knowledge about the molecular mechanism of these types of compounds. Theoretical calculations had been used successfully to consider reaction mechanisms in related systems by Safont et al.[6] and by Chuchani et al.[7] Consequently, the present work aimed at studying the potential energy surface (PES) at the Density Functional Theory (DFT) level to compare the kinetics and thermodynamic parameters to the experimental values of the eliminations (II) and (II).

II. Computational Methods and Models

The reaction path for the gas phase decomposition reaction of triethyl and trimethyl orthoacetate into the observed products, ethanol or methanol and the corresponding unsaturated ketal, was studied using electronic structure calculations. The B3LYP/6-31G(d,p), B3LYP/6-31G++(d,p), B3PW91/6-31G(d,p), B3PW91++G(d,p), MPW1PW91/6-31G(d,p), and MPW1PW91/6-31++G(d,p) levels of theory, as implemented in Gaussian 03W[8] were selected. The Berny analytical gradient optimization routines were used. The requested convergence on the density matrix was 10^{-9} atomic units, the threshold value for maximum displacement was 0.0018 Å, and that for the maximum force was 0.00045 hartree/b. Transition state searches were performed using Quadratic Synchronous Transit protocol as implemented in Gaussian 03W. The nature of stationary points was established by calculating and diagonalizing the Hessian matrix (force constant matrix). TS structures were characterized by means of normal-mode analysis. Intrinsic reaction coordinate (IRC) calculations were performed to verify transition state structures. The unique imaginary frequency associated with the transition vector (TV), i.e., the eigenvector associated with the unique negative eigenvalue of the force constant matrix, has been characterized.

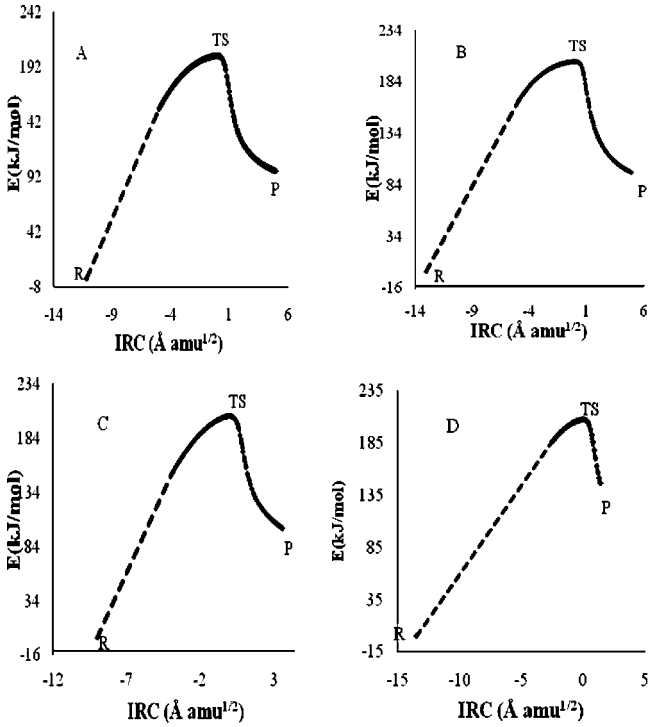

Figure 1. IRC reaction profiles for thermal decompositions of triethyl and trimethyl orthoacetate at B3LYP/6-31G** level of theory: A, triethyl orthoacetate; B, triethyl orthopropionate; C, trimethyl orthoacetate; D, trimethyl orthobutirate.

Thermodynamic quantities, such as zero point vibrational energy (ZPVE), temperature corrections $E(T)$, and absolute entropies $S(T)$, were obtained from frequency calculations, and consequently, the rate coefficient can be estimated assuming that the transmission coefficient is equal to 1. Thermal corrections and absolute entropies were obtained assuming ideal gas behavior from the harmonic frequencies and moments of inertia by standard methods[9] at average temperature and pressure values within the experimental range. Scaling factors for frequencies and zero point energies for B3LYP methods used are taken from the literature.[10] For the DFT methods, B3PW91, MPW1PW91, and the B3LYP value were used.

The first-order rate coefficient $k(T)$ was calculated using the transition state theory (TST)[11] and assuming that the transmission coefficient is equal to 1, as expressed in the following expression (eq 1)

$$k(T) = (k_B T/\hbar) \exp(-\Delta G^{\#}/RT) \quad (1)$$

where $\Delta G^{\#}$ is the Gibbs free energy change between the reactant and the transition state and k_B and $\hbar$ are the Boltzmann and Plank constants, respectively.

$\Delta G^{\#}$ was calculated using the following relations (eqs 2 and 3)

$$\Delta G^{\#} = \Delta H^{\#} - T\Delta S^{\#} \quad (2)$$

$$\Delta H^{\#} = V^{\#} + \Delta \mathrm{ZPVE} + \Delta E(T) \quad (3)$$

where $V^{\#}$ is the potential energy barrier and ΔZPVE and $\Delta E(T)$ are the differences of ZPVE and thermal corrections between the TS and the reactant, respectively. Entropy values were calculated from vibrational analysis.

III. Results and Discussions

IIIa. Kinetic and Thermodynamic Parameters. The decomposition path for the thermolysis of ethyl and methyl orthoesters to give ethanol or methanol and the corresponding unsaturated ketal was studied at different theory levels. These studies show that the mechanism involves a rate-determining step through a four-membered transition state. Essentially the same structure for TS was obtained for all theory levels. The TS structure was verified using vibrational analysis.

IRC calculations demonstrated that the TS structure connects the reactant and products in the reaction path (see Figure 1). Calculations showed that the reaction path through a four-

TABLE 1: Calculated Kinetic and Thermodynamic Parameters for the Gas Phase Elimination of Triethyl Orthoesters ($RCH_2C(OC_2H_5)_3$) at 330 °C

R	method	E_a (kJ/mol)	log A	$\Delta S^{\ddagger}$ (J/(K·mol))	$\Delta H^{\ddagger}$ (kJ/mol)	$\Delta G^{\ddagger}$ (kJ/mol)	$10^4 k_1$ (s^{-1})
H	experimental	187.6	13.76	4.3	182.6	180.0	32.5
	B3LYP/6-31G**	200.9	13.88	6.7	195.9	191.9	3.0
	B3LYP/6-31++G**	199.2	14.33	15.3	194.2	185.0	11.9
	B3PW91/6-31G**	214.8	13.62	1.6	209.8	208.8	0.1
	B3PW91/6-31++G**	206.8	14.27	14.2	201.8	193.3	2.3
	MPW1WP91/6-31G**	224.5	13.70	3.2	219.5	217.5	0.02
	MPW1WP91/6-31++G**	216.3	14.37	15.9	211.3	201.7	0.43
	fast step (B3LYP/6-31G*)	139.3	12.77	−14.5	134.3	143.0	51606
CH_3	experimental	193.3	13.63	1.8	188.3	187.2	10.0
	B3LYP/6−31G**	212.3	14.22	13.1	207.3	199.4	0.7
	B3LYP/6-31++G**	202.3	15.31	34.0	197.3	176.8	61.3
	B3PW91/6-31G**	218.6	14.18	12.3	213.6	206.2	0.2
	B3PW91/6-31G**	210.3	14.88	25.8	205.3	189.8	4.6
	MPW1WP91/6-31G**	238.8	14.16	12.1	233.8	226.5	0.002
	MPW1WP91/6-31++G**	210.1	14.44	17.3	205.1	194.7	1.7
	fast step (B3LYP/6-31G*)	125.6	12.74	−14.5	120.6	133.2	365504

TABLE 2: Calculated Kinetic and Thermodynamic Parameters for the Gas Phase Elimination of Trimethyl Orthoesters ($RCH_2C(OCH_3)_3$)at 330 °C

R	method	E_a (kJ/mol)	log A	$\Delta S^{\ddagger}$ (J/(K·mol))	$\Delta H^{\ddagger}$ (kJ/mol)	$\Delta G^{\ddagger}$ (kJ/mol)	$10^4 k_1$ (s^{-1})
H	experimental	194.7	13.58	0.1	189.7	189.6	5.2
	B3LYP/6-31G**	213.8	13.97	8.4	208.8	203.4	0.3
	B3LYP/6-31++G**	201.8	14.41	16.8	196.8	186.5	8.9
	B3PW91/6-31G**	219.5	14.02	9.4	214.5	208.7	0.1
	B3PW91/6-31++G**	209.3	14.37	15.9	204.3	194.5	1.8
	MPW1WP91/6-31G**	222.5	14.18	12.4	217.4	209.8	0.1
	MPW1WP91/6-31++G**	218.6	14.68	22.0	213.5	200.0	0.6
$CH_3CH_2CH_2$	experimental	195.3	13.97	8.4	190.3	185.2	11.3
	B3LYP/6-31G**	210.4	14.45	17.6	205.4	194.8	1.7
	B3LYP/6-31++G**	196.3	14.54	19.4	191.2	179.6	35.3
	B3PW91/6-31G**	215.7	14.59	20.2	210.7	198.6	0.8
	B3PW91/6-31G**	203.6	14.64	21.2	198.6	185.8	10.1
	MPW1WP91/6-31G**	223.5	14.05	9.8	218.4	212.5	0.1
	MPW1WP91/6-31++G**	204.8	14.89	26.0	199.8	184.1	14.2

TABLE 3: Contributions to the Entropy of Activation for Triethyl and Trimethyl Orthoacetate, at B3LYP/6-31G Level of Theory**

substrate	$\Delta S^{\ddagger}_{Rotational}$ (J/(K·mol))	$\Delta S^{\ddagger}_{Vibrational}$ (J/(K·mol))	$\Delta S^{\ddagger}_{Traslational}$ (J/(K·mol))	$\Delta S^{\ddagger}_{Total}$ (J/(K·mol))
triethyl orthoacetate	1.7	5.0	0	6.7
triethyl orthopropionate	1.5	11.6	0	13.1
trimethyl orthoacetate	2.1	6.3	0	8.4
trimethyl orthobutyrate	1.8	15.8	0	17.6

membered ring is unique to the formation of unsaturated ketal and the respective alcohol.

Calculated parameters for the thermal elimination of ethyl and methyl orthoesters are given in Tables 1 and 2. Considering the DFT methods, the B3LYP functional renders the best agreement to the experimental values. The increased basis sets did not improve calculated parameters. The functional B3PW91 also gave reasonable results. In the case of ethyl orthoesters, the product unsaturated ketal further decomposes to ethylene and the respective ethyl ester. This step was also studied at the B3LYP level and the results show that this step is much faster than the preceding one (Table 1), thus implying that the rate-

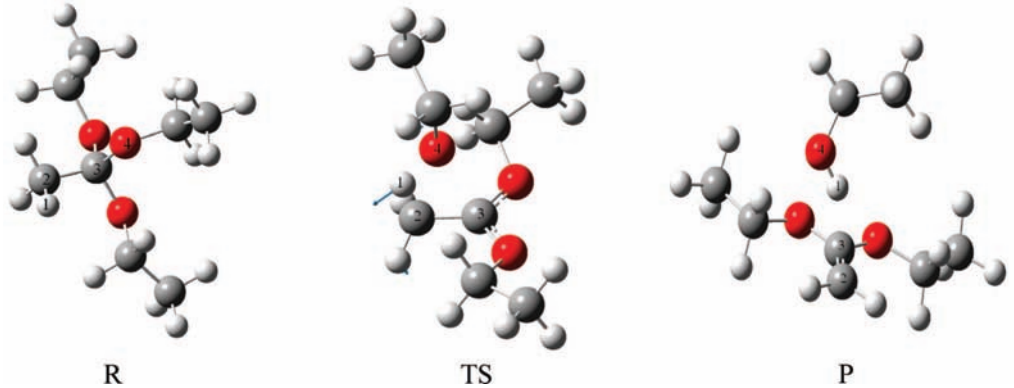

Figure 2. Optimized structures for reactant (R), transition state (TS), and products ethanol and 1.1-diethoxypropene (P) at the B3LYP/6-31G** level of theory for ethyl orthoacetate: gray balls, C; red balls, O; white balls, H. TV = transition vector.

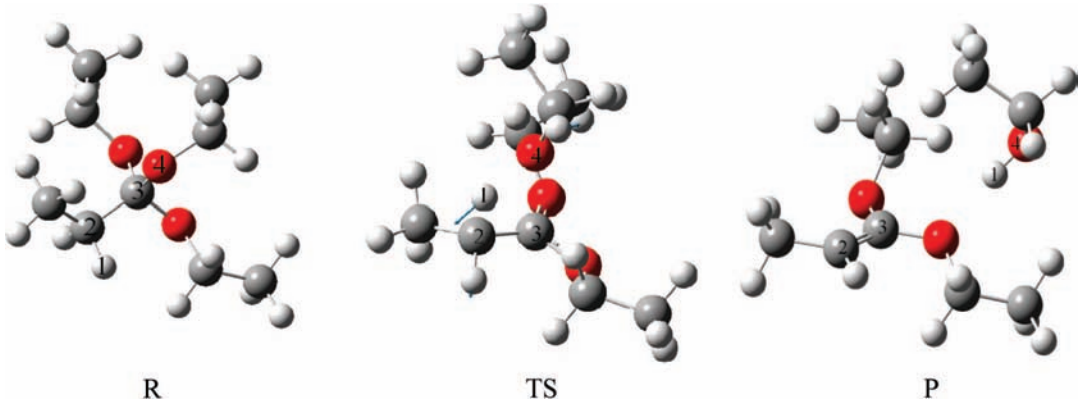

Figure 3. Optimized structures for reactant (R), transition state (TS), and products ethanol and 1.1-diethoxyethene (P) at B3LYP/6-31G** level of theory for ethyl orthopropionate: gray balls, C; red balls, O; white balls, H.

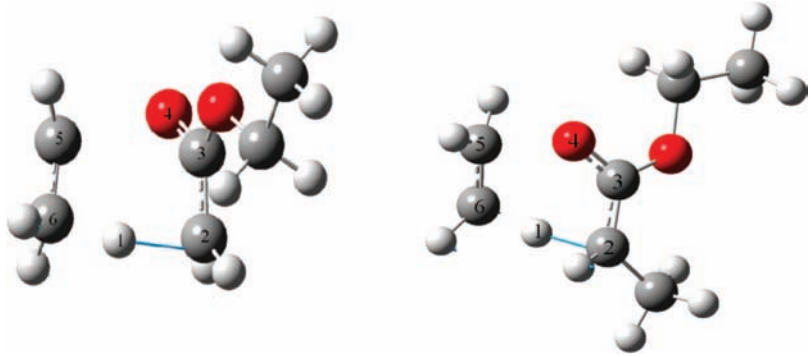

Figure 4. Optimized structures for the transition state (TS) of the fast step at B3LYP/6-31G** level of theory for ethyl orthoacetate (A) and ethyl orthopropionate (B) to produce ethylene and the corresponding carboxylic acid ester: gray balls, C; red balls, O; white balls, H.

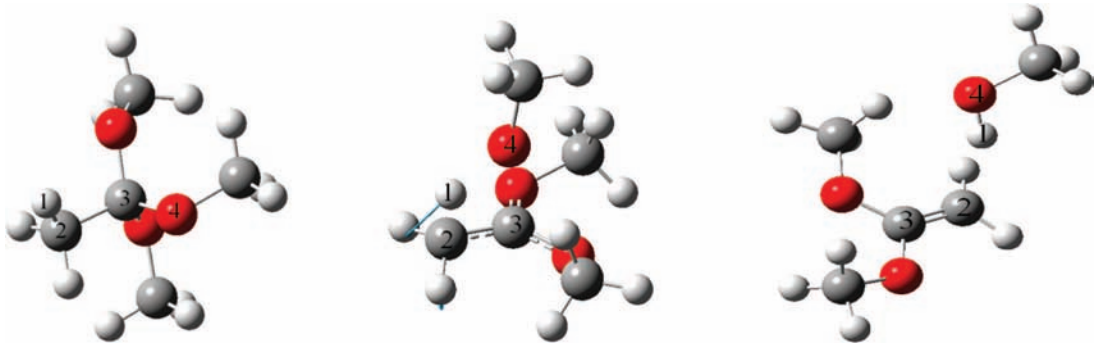

Figure 5. Optimized structures for reactant (R), transition state (TS) and products methanol and 1,1-dimethoxyethene (P) at B3LYP/6-31G** level of theory for methyl orthoacetate: gray balls, C; red balls, O; white balls, H.

determining step in this case is the decomposition of the ethyl orthoester to ethanol and the corresponding unsaturated ketal.

Values of enthalpy and entropy of activation are in good agreement for B3LYP method, and consequently, the rate constants are comparable to the experimental values. The entropy of activation for all these processes is small and positive, suggesting an increase of degrees of freedom and a fairly loose transition state configuration. Triethyl orthoesters have experimental entropies of activation of approximately 2−4 J/(K·mol) (Table 1). For the methyl orthoester when R = H the entropy of activation is very small and close to zero (0.13 J/(K·mol)). However, when R = $CH_3CH_2CH_2$, this value is more positive (8.4 J/(K·mol)) compared to the other orthoesters studied (Table 2).

To understand better the differences in entropies of activation, an analysis of the contribution of the different components was considered (Table 3). The major contribution to $\Delta S^{\ddagger}$ is the vibrational component in all substrates. Trimethyl orthobutyrate exhibits the greatest value. This is reasonable since the butyrate possess a greater number of vibrational modes.

IIIb. Transition State and Mechanism. The transition vectors linked with the imaginary frequency for the TS in the reaction studied are shown in Figures 2, 3, 5, and 6, center structure. The configuration of the TS of these reactions is a four-membered ring. The transition vector is associated with the hydrogen transfer from the carbon C_2 to the oxygen atom O_4 to form the corresponding alcohol. Structural parameters and charges for reactant orthoester (R), transition state (TS), and products (P) are given in Table 4. The imaginary frequency in these reactions ranges from 200 to 400 cm^{-1}. The TS configurations show the transference of the hydrogen to the alcoholic oxygen in the products. Dihedral angles are small implying the TS structures are almost planar.

Ethyl orthoesters undergo a consecutive rapid step decomposition to give the corresponding unsaturated ketal and ethanol. In the rapid step, the unsaturated ketal eliminates to give

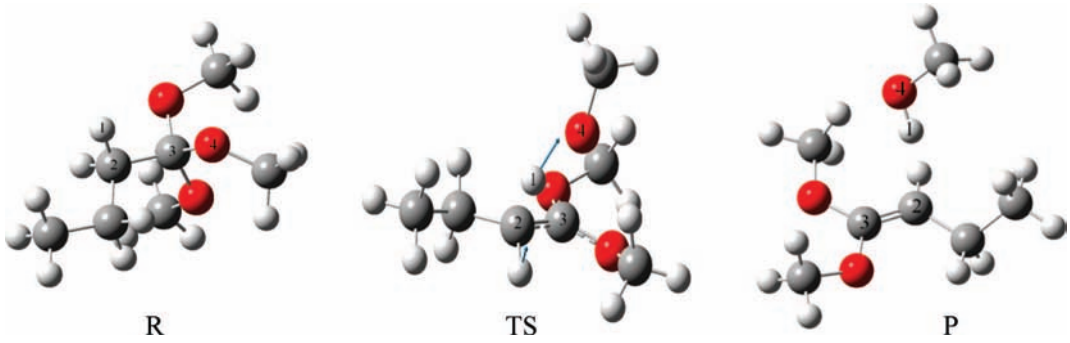

Figure 6. Optimized structures for reactant (R) transition state (TS), and products methanol and 1,1-dimethoxybutene (P) at B3LYP/6-31G** level of theory for methyl orthobutyrate: gray balls, C; red balls, O; white balls, H.

TABLE 4: Structural Parameters for Triethyl and Trimethyl Orthoesters (R) and Thermal Decompositions and the Four-Member Ring Transition States (TS) from B3LYP/6-31G Calculations**

sustrate	bond	R	ST	P
triethyl orthoacetate	H(1)−C(2)	0.91	0.62	0.03
	H(1)−O(4)	0.001	0.20	0.72
	O(4)−C(3)	0.91	0.20	3.45
	C(3)−C(2)	1.00	1.17	1.72
		dihedral angles		
	H(1)−C(2)−C(3)−O(4)	−58.95	−0.22	
	C(2)−C(3)−O(4)−H(1)	23.88	0.21	
	C(3)−O(4)−H(1)−C(2)	−36.73	−0.34	
	O(4)−H(1)−C(2)−C(3)	30.09	0.47	
	imaginary frequency	271.4 (cm^{-1})		
triethyl orthopropionate	H(1)−C(2)	1.09	1.18	3.93
	H(1)−O(4)	2.77	1.52	0.98
	0(4)−C(3)	1.44	2. 49	3.82
	C(3)−C(2)	1.53	1. 45	1.34
		dihedral angles		
	H(1)−C(2)−C(3)−O(4)	−72.58	−1.17	
	C(2)−C(3)−O(4)−H(1)	28.68	1.12	
	C(3)−O(4)−H(1)−C(2)	−44.96	−1.85	
	O(4)−H(1)−C(2)−C(3)	31.12	2.57	
	imaginary frequency	204.7 (cm^{-1})		
trimethyl orthoacetate	H(1)−C(2)	1.09	1.19	2.24
	H(1)−O(4)	2.56	1.51	0.99
	0(4)−C(3)	1.44	2.41	3.44
	C(3)−C(2)	1.52	1.44	1.35
		dihedral angles		
	H(1)−C(2)−C(3)−O(4)	−52.30	3.03	
	C(2)−C(3)−O(4)−H(1)	21.89	−2.91	
	C(3)−O(4)−H(1)−O(2)	−32.66	4.66	
	O(4)−H(1)−C(2)−C(3)	27.54	−6.41	
	imaginary frequency	407.5 (cm^{-1})		
trimethyl orthobutyrate	H(1)−C(2)	1.10	1.19	2.30
	H(1)−O(4)	2.81	1.52	0.98
	O(4)−C(3)	1.45	2.41	3.44
	C(3)−C(2)	1.53	1.45	1.35
	imaginary frequency	355.9 (cm^{-1})		
		dihedral angles		
	H(1)−C(2)−C(3)−O(4)	−68.77	0.07	
	C(2)−C(3)−O(4)−H(1)	27.50	−0.07	
	C(3)−O(4)−H(1)−C(2)	−41.50	0.11	
	O(4)−H(1)−C(2)−C(3)	29.58	−0.15	

ethylene and the corresponding ester. The TS configuration for the fast step of the unsaturated ketal is a six-membered structure (Figure 4), and the transition vector linked to the imaginary frequency is associated with the transference of hydrogen H_1 from carbon C_6 to carbon C_2 to yield ethylene, and the unique imaginary frequency is in the order of 1000 cm^{-1}.

IIIc. NBO Changes. Changes in electron distribution during the reaction can be studied by means of charges. NBO charges have proven useful in this sense. We report NBO charges for reactant, TS, and products in Table 5, atom numbering is the same as that given in Scheme 1. There is an increase of positive charge in the hydrogen being transferred H1, as the oxygen O4 increases in negative charge. Similar changes in electron density are observed for all reactants as the reaction progresses from reactant to transition states to products.

IIId. Bond Order Analysis. The reaction progress along the reaction pathway was also investigated by means of NBO bond order calculations.[12−14] Wiberg bond indexes[15] were computed using the natural bond orbital NBO program[16] as implemented in Gaussian 03W. These indexes can be used to estimate bond orders from population analysis. Bond breaking and making processes involved in the reaction mechanism are monitored

TABLE 5: NBO Charges of the Atoms Involved in the Four-Membered TS for the Reaction of Triethyl and Trimethyl Orthoesters at B3LYP/6-31G Level of Theory**

substrate	atom	R	TS	P
triethyl orthoacetate	H(1)	0.15	0.32	0.36
	C(2)	−0.42	−0.53	−0.43
	C(3)	0.63	−0.67	0.53
	O(4)	−0.53	−0.67	−0.62
triethyl orthopropionate	H(1)	0.14	0.31	0.41
	C(2)	0.64	0.67	−0.51
	C(3)	−0.53	−0.38	0.12
	O(3)	−0.51	−0.66	−0.65
trimethyl orthoacetate	H(1)	0.17	0.32	0.37
	C(2)	−0.39	−0.51	−0.42
	C(3)	0.62	0.68	0.60
	O(4)	−0.54	−0.67	−0.63
trimethyl orthobutyrate	H(1)	0.16	0.32	0.37
	C(2)	−0.23	−0.37	−0.20
	C(3)	0.63	0.69	0.55
	O(4)	−0.54	−0.67	−0.64

SCHEME 1

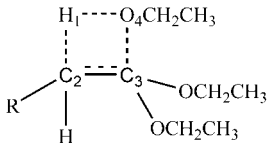

R = H, Mc

Triethyl orthoesters

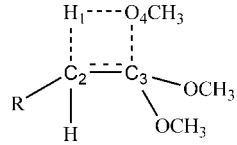

R = H, Pr

Trimethyl orthoester

by means of the synchronicity (Sy) concept proposed by Moyano et al.[17] defined by the expression (eq 4)

$$\mathrm{Sy} = 1 - \left[\sum_{i=1}^{n} |\delta B_i - \delta B_{\mathrm{av}}| \delta B_{\mathrm{av}}\right] \Big/ 2n - 2 \qquad (4)$$

*n*is the number of bonds directly involved in the reaction and the relative variation of the bond index is obtained from eq 5a

$$\delta B_i = [B_i^{\mathrm{TS}} - B_i^{\mathrm{R}}]/[B_i^{\mathrm{P}} - B_i^{\mathrm{R}}] \qquad (5a)$$

where the superscripts R, TS, and P represent reactant, transition state, and product, respectively.

The evolution in bond change is calculated as in eq 6

$$\%\mathrm{Ev} = \delta B_i{}^{*}100 \qquad (6)$$

The average value is calculated from eq 7

$$\delta B_{\mathrm{ave}} = 1/n \sum_{i=1}^{n} \delta Bi \qquad (7)$$

The reaction changes along the reaction coordinate can be followed using Wiberg bonds indexes B_i. The analysis was performed for the decomposition of ethyl orthoesters (rate-determining step) and methyl orthoesters. The indexes were calculated for the bonds involved in the reaction changes, i.e., H_1-C_2, C_2-C_3, C_3-O_4, and O_4-H_1 (Scheme 1 and Table 6), since changes in all other bond bonds are practically negligible during the process. Atom numbering for structural parameters (atom distances, dihedral angles) and NBO calculations are shown in Scheme 1.

Bond order analysis shows that the decomposition process is dominated by the elongation of bond C_3-O_4, with 77−80% progress in the transition state. The TS however is early in the progress of other reaction coordinates (23−34%). Nonetheless, the small differences in the reaction progress and charge development in the TS suggest that the reaction is more asyncronic for the decomposition of ethyl orthoesters with synchronicity values Sy = 0.68 and 0.77, when compared to methyl orthoesters with synchronicity values of Sy = 0.90.

IV. Conclusions

The DFT theoretical calculations carried out on the thermal decomposition of ethyl and methyl orthoesters were in good agreement with the experimental values. These results support a four-membered cyclic transition state type of mechanism. In the case of ethyl orthoesters, the corresponding unsaturated ketal undergoes a very rapid six-membered cyclic transition state decomposition to give ethylene and the corresponding ethyl ester. The triethyl orthoesters elimination was shown to be more polar (Sy = 0.68 and 0.77) than the trimethyl orthoesters (Sy = 0.90 for both substrates). This fact suggests that the ethoxy group is a better leaving group than the methoxy group.

TABLE 6: Wiberg Bond Indexes for the Thermal Decompositions of Triethyl and Trimethyl Orthoesters, from B3LYP/6-31G Calculations**

substrate	bond	R(B_i)	TS(B_i)	P(B_i)	%Ev	ΔB_{av}	S_y
triethyl orthoacetate	H(1)−C(2)	0.91	0.62	0.03	32.8	0.40	0.68
	C(2)−C(3)	1.00	1.17	1.72	23.1		
	C(3)−O(4)	0.91	0.20	0.01	78.7		
	H(1)−O(4)	0.001	0.20	0.72	27.0		
triethyl orthopropionate	H(1)−C(2)	0.90	0.61	0.002	32.7	0.50	0.77
	C(2)−C(3)	0.98	1.15	1.79	20.7		
	C(3)−O(4)	0.91	0.20	0.002	79.9		
	O(4)−H(1)	0.001	0.19	0.69	26.4		
trimethyl orthoacetate	H(1)−C(2)	0.92	0.61	0.03	34.4	0.41	0.90
	C(2)−C(3)	1.003	1.18	1.73	24.3		
	C(3)−O(4)	0.91	0.22	0.01	76.7		
	O(4)−H(1)	0.001	0.20	0.71	27.8		
trimethyl orthobutyrate	H(1)−C(2)	0.89	0.60	0.03	34.0	0.41	0.90
	C(2)−C(3)	0.99	1.16	1.71	24.6		
	C(3)−O(4)	0.92	0.22	0.01	77.3		
	O(4)−H(1)	0.001	0.20	0.72	27.4		

Acknowledgment. T.C. is grateful to the Consejo de Desarrollo Científico y Humanístico (C.D.C.H.) for Grant No. PG-03-00-6499-2006.

References and Notes

(1) Staudinger, H.; Rathsam, G. *Helv. Chim. Acta* **1922**, *5*, 645–655, and references cited therein.

(2) McElvain, S. M.; Anthes, H. I.; Shapiro, S. H. *J. Am. Chem. Soc.* **1942**, *64*, 2525–2531.

(3) McElvain, S. M.; Stevens, C. L. *J. Am. Chem. Soc.* **1946**, *68*, 1917–1961.

(4) Marquez, E.; Tosta, M.; Domínguez, R. M.; Herize, A.; Chuchani, G. *J. Phys. Org. Chem.* **2008**, *21*, 666–669.

(5) Marquez, E.; Dominguez, R. M.; Tosta, M.; Chuchani, G. *J. Phys.Chem. A* **2008**, *112*, 12140–12142.

(6) (a) Safont, V. S.; Moliner, V.; Andres, J.; Domingo, L. R. *J. Phys. Chem. A* **1997**, *101*, 1859–1865. (b) Safont, V. S.; Andres, J.; Castillo, R.; Chuchani, G.; Rotinov, A.; Domínguez, R. M.; Herize, A. *J. Phys. Chem. A* **2004**, *108*, 996–1007.

(7) (a) Mora, J. R.; Tosta, M.; Domínguez, R. M.; Herize, A.; Barroso, J.; Córdova, T.,; Chuchani, G. *J. Phys. Org. Chem.* **2007**, *20*, 1021–1031. (b) Herize, A.; Mora, J. R.; Lezama, J.; Marquez, E.; Córdova, T.; Chuchani, G. *J. Phys. Org. Chem.* **2009**, *22*, 170–176.

(8) Frisch, M. J.; Trucks, G. W.; Schlegel, H. B.; Scuseria, G. E.; Robb, M. A.; Cheeseman, J. R.; Montgomery, J. A., Jr.; Vreven, T.; Kudin, K. N.; Burant, J. C.; Millam, J. M.; Iyengar, S. S.; Tomasi, J.; Barone, V.; Mennucci, B.; Cossi, M.; Scalmani, G.; Rega, N.; Petersson, G. A.; Nakatsuji, H.; Hada, M.; Ehara, M.; Toyota, K.; Fukuda, R.; Hasegawa, J.; Ishida, M.; Nakajima, T.; Honda, Y.; Kitao, O.; Nakai, H.; Klene, M.; Li, X.; Knox, J. E.; Hratchian, H. P.; Cross, J. B.; Bakken, V.; Adamo, C.; Jaramillo, J.; Gomperts, R.; Stratmann, R. E.; Yazyev, O.; Austin, A. J.; Cammi, R.; Pomelli, C.; Ochterski, J. W.; Ayala, P. Y.; Morokuma, K.; Voth, G. A.; Salvador, P.; Dannenberg, J. J.; Zakrzewski, V. G.; Dapprich, S.; Daniels, A. D.; Strain, M. C.; Farkas, O.; Malick, D. K.; Rabuck, A. D.; Raghavachari, K.; Foresman, J. B.; Ortiz, J. V.; Cui, Q.; Baboul, A. G.; Clifford, S.; Cioslowski, J.; Stefanov, B. B; Liu, G.; Liashenko, A.; Piskorz, P.; Komaromi, I.; Martin, R. L.; Fox, D. J.; Keith, T.; Al-Laham, M. A.; Peng, C. Y.; Nanayakkara, A.; Challacombev, M.; Gill, P. M. W.; Johnson, B.; Chenv, W; Wong, M. W.; Gonzalez, C.; Pople, J. A. *Gaussian 03, Revision C.02*; Gaussian, Inc.: Wallingford, CT, 2004.

(9) McQuarrie, D. *Statistical Mechanics*; Harper & Row: New York, 1986.

(10) Foresman, J. B.; Frisch, Æ. *Exploring Chemistry with Electronic Structure Methods*, 2nd ed.; Gaussian, Inc.: Pittsburgh, PA, 1996.

(11) Benson, S. W. *The Foundations of Chemical Kinetics*; Mc-Graw-Hill: New York, 1960.

(12) Lendvay, G. L. *J. Phys. Chem.* **1989**, *93*, 4422–4429.

(13) Reed, A. E.; Weinstock, R. B.; Weinhold, F. *J. Chem. Phys.* **1985**, *83* (2), 735–746.

(14) Reed, A. E.; Curtiss, L. A.; Weinhold, F. *Chem. Rev.* **1988**, *88*, 899–926.

(15) Wiberg, K. W. *Tetrahedron* **1968**, *24*, 1083–1095.

(16) Reed, A. E., Carpenter, J. E., Weinhold, F. *NBO version 3.1*.

(17) Moyano, A.; Pericás, M. A.; Valenti, E. *J. Org. Chem.* **1989**, *54*, 573–582.

JP8108336